A High-Efficiency ASK-Modulated Class-E Power and Data Transmitter for Medical Implants

Mohammad Mahdi Ahmadi, *Senior Member, IEEE*, Shirin Pezeshkpour, *Student Member, IEEE*, and Zahra Kabirkhoo, *Student Member, IEEE*

***Abstract*—In this article, we propose an amplitude-shift keying (ASK) modulation technique for Class-E power transmitters used in the inductive power and data transfer links. The proposed modulation circuit consists of a capacitor and a transistor, which switch the load network of the Class-E transmitter between two states; in one state, the drain waveform of the Class-E transistor satisfies both zero-voltage switching (ZVS) and zero-voltage-derivative switching conditions, while in the other one, the waveform approximately satisfies the ZVS condition. Therefore, at both states, the dc-to-ac power conversion efficiency is high, but the transmitted power is different, which allows the implementation of ASK data modulation in the transmitter. We also present an analytical procedure to design the circuit for the desired output power and data modulation index (MI). We have verified the design procedure in both simulation and measurement. The implemented inductive link consists of a 2.4-μH transmitter coil and a 1.1-μH receiver coil, separated by a 10-mm air gap. With a carrier frequency of 10 MHz, the power transfer efficiency and the power delivered to load were measured to be 64.6% and 35 mW, respectively. With MI = 10%, the bit error rate for the data rates of 1 and 2 Mb/s was measured to be less than 10^{-8} and 10^{-6}, respectively.**

***Index Terms*—Amplitude-shift keying (ASK), Class-E power transmitter, data transmission, inductive link, medical implant, wireless power transfer.**

I. Introduction

INDUCTIVE links are widely used to transfer power to smart medical implants, such as artificial pacemakers [1], [2], cochlear implants [3]–[5], retinal prostheses [6]–[9], deep brain stimulators [10], [11], and spinal cord stimulators [12]–[14]. Along with power, these links are also used to transmit data to medical implants that are used to apply artificially acquired sensory information to the central or peripheral nervous systems. The rate of data transmission to this type of implants should be sufficiently high, e.g., more than 1 Mb/s for cochlear implants [5], [15] and 20 Mb/s or more for visual prostheses [9], [15].

Amplitude-shift keying (ASK) is commonly used to transmit data to inductively-powered medical implants. ASK is attractive because of its fairly simple circuit implementation. Also, in ASK, the frequency of the power carrier signal is fixed and information is transmitted by modulating the amplitude of the carrier signal; this allows tuning the receiver *LC* tank to the power carrier frequency, which, in turn, maximizes the power transfer efficiency (PTE) of the link [16].

Inductive power transfer links are driven by either Class-D or Class-E power transmitters. For driving inductive power transfer links used for medical implants, Class-E transmitters are preferred over the Class-D ones [17] because these links often work at high frequencies (HF band), and at those frequencies, the power loss for charge/discharge of the parasitic capacitors of the switches becomes larger in a Class-D transmitter compared with that of a Class-E one.

A Class-E power amplifier (PA) or power transmitter can be nearly 100% efficient, if it is *nominally tuned*, which means it satisfies zero-voltage switching (ZVS) and zero-voltage-derivative switching (ZVDS) conditions [18]. For each Class-E power transmitter, with a specific power supply and at a specific operating frequency, there is only a single set of component values that makes the power transmitter nominally tuned. In such a case, the amplitude of the voltage across the transmitter coil is constant and proportional to the supply voltage. However, to implement ASK modulation, the amplitude of the voltage across the transmitter coil should change according to the input data bit. If one wants to keep the power transmitter nominally tuned at both data modulation states, one should either modulate the power supply of the transmitter [19], or modify the entire load network of the transmitter [20]. Either of these approaches results in reduced PTE in one of the data modulation states [20].

It is known that a Class-E PA does not necessarily need to be nominally tuned to provide high efficiencies [21]. In fact, in a practical Class-E PA, whose switching transistor has a nonzero ON-resistance, the highest efficiency is often obtained if the switch voltage at the turn-on time is slightly greater than zero [22]. This phenomenon was the reason that Nathan Sokal, the inventor of Class-E PA, changed the term *optimally-tuned* to *nominally-tuned* for a PA satisfying ZVS and ZVDS conditions [23].

We study the foregoing feature of a Class-E PA in Section II of this article and introduce an ASK-modulated Class-E power transmitter that can provide very high efficiencies in both of its modulation states. In Section III, we propose an empirical formula for relating the output power of a Class-E PA to its load network angle. In Section IV, we take advantage of the

Manuscript received January 28, 2021; revised April 21, 2021 and June 10, 2021; accepted June 18, 2021. Date of publication June 28, 2021; date of current version September 16, 2021. This work was supported in part by the Cognitive Sciences and Technologies Council of Iran under Grant 3738. Recommended for publication by Associate Editor C. K. Tse. *(Corresponding author: Mohammad Mahdi Ahmadi.)*

The authors are with the Department of Biomedical Engineering, Amirkabir University of Technology, Tehran 15875-4413, Iran (e-mail: mmahmadi@aut.ac.ir; sh.pezeshkpour@aut.ac.ir; kabiri1373@aut.ac.ir).

Color versions of one or more figures in this article are available at https://doi.org/10.1109/TPEL.2021.3092829.

Digital Object Identifier 10.1109/TPEL.2021.3092829

proposed formulas in Section III and prescribe an analytical procedure to design the proposed circuit for a desired output power and data modulation index (MI). We demonstrate the feasibility of the proposed circuit and its design procedure in Section V. In Section VI, we present a prototyped inductive power and data transfer link designed based on the proposed design procedure. The built prototype achieves a PTE of 64.6%, which is considerably larger than that of any previously-reported circuit. The bit error rate (BER) of the link for the data rates of 1 and 2 Mb/s was measured to be less than 10^{-8} and 10^{-6}, respectively.

II. Theory of Operation

A. Overview of Class-E Power Transmitters

Fig. 1(a) illustrates a basic schematic of an inductive link driven by a Class-E PA. In Fig. 1(a), transistor M_1 acts as a switch and is periodically turned on and off by a clock signal. The RF choke $L_{\rm RFC}$ has a high impedance at the operating frequency, behaving as a constant dc current source. When M_1 is ON, $L_{\rm RFC}$ is placed between $V_{\rm DD}$ and ground, gaining energy from $V_{\rm DD}$. When M_1 turns off, $L_{\rm RFC}$ pumps the gained energy from $V_{\rm DD}$ into the load network of the PA. $L_{\rm t}$ and $L_{\rm r}$ are the transmitter and receiver coils, respectively. The parasitic series resistances (ESRs) of $L_{\rm t}$ and $L_{\rm r}$ are represented by $R_{\rm Lt}$ and $R_{\rm Lr}$, respectively. $C_{\rm r}$ is a capacitor that resonates with $L_{\rm r}$ at $\omega_{\rm c}$, and finally, $R_{\rm L}$ is a resistance representing the power dissipation in the implant.

Usually, the values of $C_{\rm p}$ and $C_{\rm t}$ are adjusted to make the PA nominally tuned. The state of tuning is defined by the relative phase of the gate signal ($V_{\rm G}$) and the drain signal ($V_{\rm D}$) of M_1. The transistor current ($I_{\rm D}$) as well as $V_{\rm G}$ and $V_{\rm D}$ in a nominally-tuned Class-E PA are shown in Fig. 1(b). In a nominally-tuned Class-E PA, when M_1 turns on, $V_{\rm D}$ and its slope drop to zero. Under this condition, it is said that the PA satisfies ZVS and ZVDS conditions.

The reason for the ZVS condition is to guarantee that the charge stored on $C_{\rm p}$ is completely sunk by the load network before being discharged by M_1 to ground, and the reason for ZVDS is to minimize the sensitivity of the circuit to the jitter of the clock and the rise time of $V_{\rm G}$.

It can be shown that if $C_{\rm r}$ resonates with $L_{\rm r}$ at $\omega_{\rm c}$, i.e., $C_{\rm r}\ L_{\rm r} = \omega_{\rm c}^{-2}$, the circuit shown in Fig. 1(a) can be simplified to Fig. 1(c), where $R_{\rm ref}$ and $L_{\rm ref}$ represent the loading effects of the implant on the Class-E transmitter [24]. If the coupling coefficient between $L_{\rm t}$ and $L_{\rm r}$ is represented by k, the values of $R_{\rm ref}$ and $L_{\rm ref}$ can be calculated using [20]

$$R_{\rm ref} = \frac{k^2 L_{\rm t} L_{\rm r} \omega_{\rm c}^2}{R_{\rm Lr} + \frac{(L_{\rm r}\omega_{\rm c})^2}{R_{\rm L}}} \tag{1}$$

and [24]

$$L_{\rm ref} = -k^2 L_{\rm t} \tag{2}$$

respectively. Let us define the phase of the series resonant branch consisting of $C_{\rm t} - L_{\rm eff} - R_{\rm eff}$ in Fig. 1(c) by ψ. ψ can be

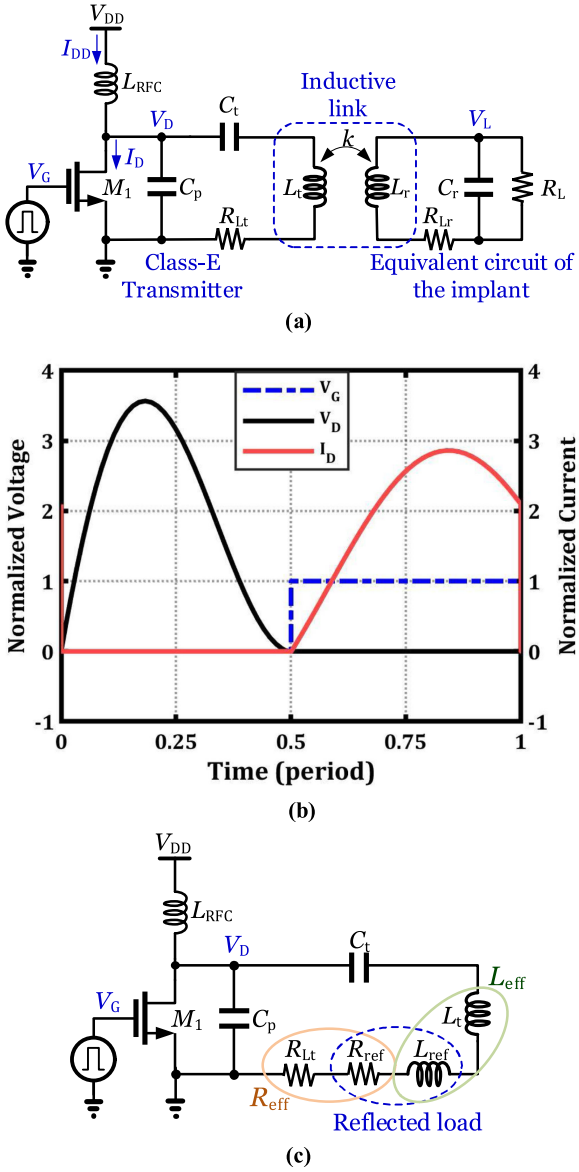

Fig. 1. (a) Schematic of a Class-E PA driving an inductive power transfer link. (b) Steady-state waveforms of the drain voltage and the gate voltage (normalized to $V_{\rm DD}$) and the drain current (normalized to $I_{\rm DD}$) of a nominally-tuned Class-E PA. (c) Simplified circuit model by reflecting the load of the implant to the transmitter circuit.

calculated using [21]

$$\psi = \tan^{-1}\left(\frac{L_{\rm eff}\omega_{\rm c} - (C_{\rm t}\omega_{\rm c})^{-1}}{R_{\rm eff}}\right) \tag{3}$$

where

$$R_{\rm eff} = R_{\rm ref} + R_{\rm Lt}, \tag{4}$$

$$L_{\rm eff} = L_{\rm ref} + L_{\rm t} = \left(1 - k^2\right) L_{\rm t}, \tag{5}$$

and $\omega_{\rm c}$ is the operating frequency in rad/s.

It is shown in [21] that, in a nominally-tuned Class-E PA whose gate drive signal has a duty ratio of $D = 0.5$, ψ is

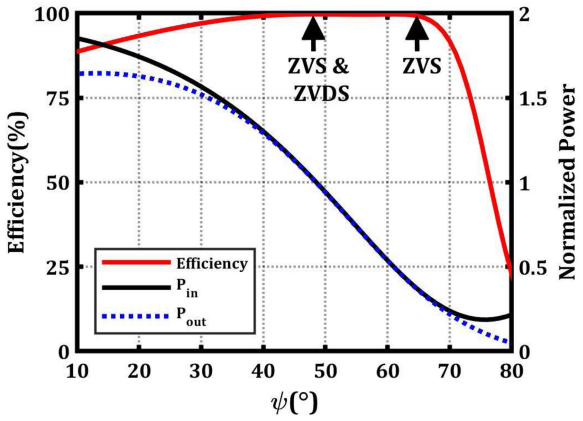

Fig. 2. Efficiency and the normalized input and output powers versus ψ for a typical Class-E power transmitter with $D = 0.5$, $Q_{\rm L} = 10$, and $L_{\rm RFC}/L_{\rm eff} = 2$. The input and output powers are normalized to the output power when the PA is nominally tuned.

approximately 49°, and the power delivered to $R_{\rm eff}$ is

$$P_{\rm t} = \frac{8}{\pi^2 + 4} \frac{V_{\rm DD}^2}{R_{\rm eff}}. \tag{6}$$

In a nominally-tuned Class-E PA, the value of ψ slightly depends on the q-factor $Q_{\rm L}$ $(= \omega_{\rm c} L_{\rm eff}/R_{\rm eff})$ and the ratio of $L_{\rm RFC}/L_{\rm eff}$. For example, for a nominally-tuned Class-E PA with $Q_{\rm L} = 10$ and $L_{\rm RFC}/L_{\rm eff} = 2$, the value of ψ is about 48°, while for a nominally-tuned Class-E PA with $Q_{\rm L} = 5$ and $L_{\rm RFC}/L_{\rm eff} = 10$, the value of ψ is about 51°.

If we sweep ψ by changing either $C_{\rm t}$ or $L_{\rm eff}$, and plot the efficiency, the normalized input power $P_{\rm in}$, and the normalized output power $P_{\rm out}$ versus ψ, we obtain curves similar to the ones plotted in Fig. 2. In this figure, $P_{\rm in}$ and $P_{\rm out}$ are normalized to the output power of the nominally-tuned PA. These curves are obtained for an exemplary Class-E PA with $Q_{\rm L} = 10$ and $L_{\rm RFC}/L_{\rm eff} = 2$; however, for other $Q_{\rm L}$ and $L_{\rm RFC}/L_{\rm eff}$ values, the curves are very similar, especially in the range from $\psi = 40°$ to $\psi = 65°$.

Fig. 2 illustrates a key point that the efficiency of a Class-E PA is close to its maximum when ψ is in the range from 40° to 65°, but $P_{\rm out}$ drops as ψ increases [21]. We can take advantage of this phenomenon and propose an ASK-modulated Class-E power transmitter that has high efficiencies at both of its modulation states. It should be noted that in a Class-E PA, at only a single ψ, both ZVS and ZVDS are truly satisfied and we call it ψ_0. There is another ψ at which only ZVS is satisfied. For the exemplary Class-E PA which we simulated for Fig. 2, at $\psi = 48°$, both ZVS and ZVDS are satisfied and at $\psi = 64.6°$, only ZVS is. In other ψ values between 40° and 65°, none of these conditions are completely satisfied, but the drain voltage is close to zero at the turn-on time of M_1. As a result, when M_1 turns on, it wastes negligible power.

As is seen in (6), in a nominally-tuned Class-E PA, the output power is proportional to $V_{\rm DD}^2$. Hence, if we change $V_{\rm DD}$ according to the input data bit, the transmitted power to the implant would change. This is the idea behind the conventional ASK-modulated Class-E power transmitters [19], [25]; however, modulating $V_{\rm DD}$ causes significant power loss in the voltage regulator that generates $V_{\rm DD}$ [20].

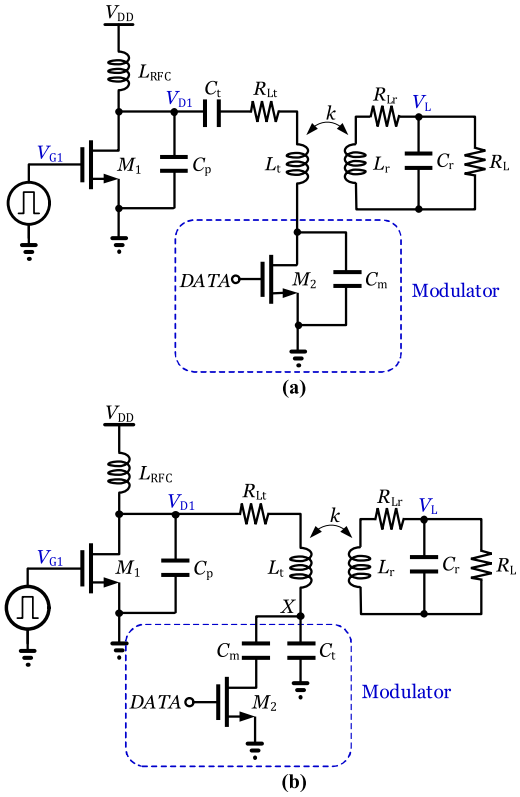

Fig. 3. Modulating the load network angle (ψ) of the transmitter by switching $C_{\rm t}$ in (a) series structure and (b) parallel structure.

B. Proposed Circuit

In ASK modulation, the amplitude of the carrier signal changes depending on the data bit. Therefore, to implement ASK modulation in a Class-E transmitter, the voltage or the current of the transmitter coil should change with the data bit. We observed in Section II-A that when ψ is between 40° and 65°, the efficiency of the PA is close to 100%. Let us define this region $(40° < \psi < 65°)$ as the *high-efficiency* region. We also observed in Fig. 2 that both $P_{\rm out}$ and $P_{\rm in}$ drop linearly with ψ in the high-efficiency region. We take advantage of this phenomenon and propose a Class-E transmitter that has high efficiency in both of its data modulation states.

To implement the foregoing idea, several schemes can be used, including (a) switching $L_{\rm t}$, (b) switching $C_{\rm t}$, or (c) switching $R_{\rm t}$. Switching $R_{\rm t}$ is not desirable because, similarly to the method proposed in [20], it introduces a resistor in the load network that degrades the efficiency. Switching $L_{\rm t}$ requires adding an extra inductor to the load network, but this is not desirable because inductors are usually large. Therefore, we resort to switching $C_{\rm t}$ as it appears to be more practical.

Fig. 3 shows two circuits to implement the proposed idea. In Fig. 3(a), when DATA is high, the terminals of $C_{\rm m}$ is shorted, and $C_{\rm t}$ constitutes the total capacitance in the series resonant branch. When DATA is low, M_2 is OFF, and the total capacitance

in the series resonant branch would be $C_tC_m/(C_t + C_m)$. The values of C_t and C_m can be chosen to keep ψ in the high-efficiency region.

The circuit depicted in Fig. 3(a) has two issues that reduce its efficiency. First, M_2 inevitably has an ON-resistance, which appears in series with $C_t - L_t$ and dissipates power when M_2 is ON. Second, when M_2 is OFF, the drain node of M_2 should be able to swing below ground; but when this node goes below ground by more than 0.7 V, the body diode of M_2 turns on and starts passing current. This issue is well explained in [16].

Fig. 3(b) shows another possible approach to switch C_t. In this circuit, when DATA is low, C_m is removed from the load network and the circuit works in its nominal Class-E operation. On the other hand, when DATA is high, C_m is placed in parallel with C_t, causing the effective capacitance in the series resonant branch as well as ψ to increase. By properly choosing the value of C_m, we can implement ASK modulation in the Class-E power transmitter while keeping the transmitter in its high-efficiency region.

The circuit of Fig. 3(b) has similar issues as the one shown in Fig. 3(a). The simulation results indicate that, for small MIs, i.e., for MI $< 6\%$, both circuits perform almost equally. For larger MIs, Fig. 3(b) achieves higher efficiencies because the side-effects of the body-diode and the ON-resistance of M_2 are much less compared with the one shown in Fig. 3(a). In the circuit of Fig. 3(b), only a portion of the current in the series resonant branch passes through these parasitic devices, while in the circuit shown in Fig. 3(a), the entire current passes through these parasitic devices.

III. Relation between P_{out} and ψ

To the best of our knowledge, to date, no formula has been proposed relating P_{out} to ψ in the high-efficiency region. Here, we develop an empirical relation between P_{out} and ψ. Fig. 4(a) plots the normalized P_{out} versus ψ for four different combinations of Q_L and L_{RFC}/L_{eff} values for the Class-E PA shown in Fig. 1(c). P_{out} is normalized to $P_{out}(\psi_0)$, which is the output power when the PA is nominally tuned and its value can be calculated using (6). Note that ψ_0 is different for each combination of Q_L and L_{RFC}/L_{eff}, and for each combination, the value of ψ_0 is a point at which normalized P_{out} is equal to one.

As is clear in Fig. 4(a), the normalized P_{out} drops almost linearly with ψ, but the line equation is different for different Q_L and L_{RFC}/L_{eff} values. In Fig. 4(b), we have plotted the normalized P_{out} versus $\tan(\psi)$ for the same combination of Q_L and L_{RFC}/L_{eff} values. In this figure, we have four different curves with different equations, but it seems that an e^{-x} relation exists between the normalized P_{out} and $\tan(\psi)$. We model this relation using

$$\frac{P_{out}(\psi)}{P_{out}(\psi_0)} = A\exp(-\tan(\psi)) \tag{7}$$

where A is a coefficient that depends on Q_L and L_{RFC}/L_{eff} and equals $\exp(\tan(\psi_0))$. If, in (7), we substitute $\exp(\tan(\psi_0))$ for A, we arrive to

$$\frac{P_{out}(\psi)}{P_{out}(\psi_0)} = \exp(\tan(\psi_0) - \tan(\psi)). \tag{8}$$

To show that (8) is a generic equation and is valid for any combination of Q_L and L_{RFC}/L_{eff}, we have plotted the normalized P_{out} versus $\exp(\tan(\psi_0) - \tan(\psi))$ for the same combinations of Q_L and L_{RFC}/L_{eff}. Clearly, all the curves are on the top of each other. This validates the assumption that the normalized P_{out} has an e^{-x} relation with $\tan(\psi)$.

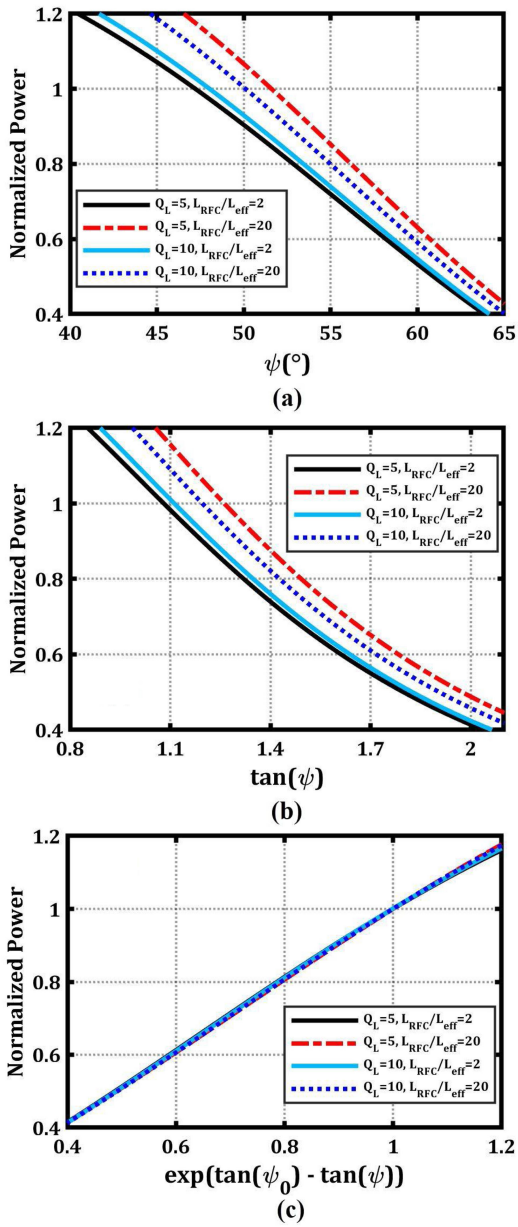

Fig. 4. (a) Normalized P_{out} ($P_{out}(\psi)/P_{out}(\psi_0)$) versus ψ, (b) normalized P_{out} versus $\tan(\psi)$, and (c) normalized P_{out} versus $\exp(\tan(\psi_0) - \tan(\psi))$ in the high-efficiency region for four different combinations of Q_L and L_{RFC}/L_{eff}.

TABLE I
TRANSMITTER AND RECEIVER INDUCTOR CHARACTERISTICS

Parameter	VALUE	Comment
L_t	2.4 μH	Transmitter coil inductance
d_t	32.4 mm	Outer diameter of transmitter coil
N_t	11	Turn number of transmitter coil
S_t	450 μm	Turn spacing of transmitter coil
W_t	700 μm	Turn width of transmitter coil
L_r	1.1 μH	Receiver coil inductance
d_r	25 mm	Outer diameter of receiver coil
N_r	8	Turn number of receiver coil
S_r	450 μm	Turn spacing of receiver coil
W_r	670 μm	Turn width of receiver coil
t	70 μm	Conductor thickness
d	10 mm	Distance between the coils

IV. DESIGN PROCEDURE

In this section, we prescribe a design procedure to find the values of the circuit components of the Class-E transmitter shown in Fig. 3(b). We explain this procedure for a Class-E power transmitter suitable for a cochlear implant, but it can be easily adopted for any ASK-modulated Class-E power and data transmitter.

The power consumption of presently used cochlear implants ranges from 20 to 40 mW [4]. Therefore, we make an assumption that our target implant requires a minimum power of 30 mW. We also assume that the implant needs a supply voltage of 5.0 V. If we assume a 2.0 V voltage drop across the voltage rectifier and the voltage regulator in the implant, the amplitude of the induced voltage across the receiver *LC* tank should be about 7.0 V. Therefore, we can model the active power consumption in the implant with a resistor R_L equal to $817\ \Omega$ ($\approx 7^2/(2\times 30\times 10^{-3})$).

The value of C_r is chosen such that C_r resonates with L_r at ω_c. Let us choose the power carrier frequency equal to 10 MHz [15], [20], [27]. To calculate the value of C_r, we should know the value of L_r at 10 MHz. Generally, the size and the geometrical specifications of L_t and L_r are selected based on the target application [28]. We targeted this exemplary inductive link for a cochlear implant. L_t and L_r, for our design example, are the planar spiral coils implemented on printed circuit boards (PCBs) and their specifications are listed in Table I.

We implemented L_t and L_r and measured their inductances to be 2.4 and $1.1\,\mu$H, and their ESRs at 10 MHz to be 0.87 and $0.54\,\Omega$, respectively. We assumed a 10-mm gap between the coils, which resulted in a measured coupling coefficient of $k = 0.21$. The value of C_r, to generate resonance in the receiver *LC* tank, is calculated to be 230.3 pF.

When DATA is low, the Class-E transmitter is nominally tuned, and the values of C_t and C_p can be calculated using the following formulas taken from [18]:

$$C_p = \frac{8}{\pi\left(\pi^2+4\right)}\ \frac{1}{\omega_c R_{\text{eff}}} \approx \frac{0.184}{\omega_c R_{\text{eff}}}, \tag{9}$$

$$C_t = \frac{1}{\omega_c R_{\text{eff}}}\left(Q_L - \frac{\pi\left(\pi^2-4\right)}{16}\right)^{-1} = \frac{1}{\omega_c R_{\text{eff}}\left(Q_L - 1.1525\right)}. \tag{10}$$

R_{ref} is calculated from (1) to be $72.0\ \Omega$, which results in $R_{\text{eff}} = R_{Lt} + R_{\text{ref}} = 72.9\,\Omega$. Using (9) and (10), we calculate the values of C_p and C_t to be 40 and 264.7 pF, respectively.

In a general-purpose Class-E PA, the value of L_{RFC} is chosen to be much larger than that of L_t[22]; however, this significantly reduces the data rate [16], [29], [30]. Therefore, we chose the value of L_{RFC} to be $6.0\ \mu$H, which is only 2.5 times larger than the value of L_t.

Now, we explain the procedure to calculate the value of C_m. As we will see later in this section, the value of C_m depends on the value of C_t, while the value of C_t, calculated using (10), is not very accurate. Therefore, we should simulate the designed Class-E transmitter, with the receiver circuit included, and fine-tune the values of C_p and C_t using the procedure explained in [22]. We used LTSPICE XVII to simulate the Class-E transmitter and fine-tune the values of C_p and C_t. This step resulted in the values of C_p and C_t to be 78 and 220 pF, respectively.

Let us assume that when DATA is low, the load network angle is ψ_0 and when DATA is high, the load network angle is ψ_1. When DATA is low, the capacitance in the series resonant branch of the Class-E transmitter only consists of C_t and we can calculate ψ_0 from (3). In order to calculate ψ_1, we assume

$$C_m = \alpha C_t \tag{11}$$

where α is the ratio of the C_m over C_t. ψ_1 is the load network angle when the total capacitance in the series resonant branch is $C_m + C_t$. Substituting C_t in (3) with $C_m + C_t$, and taking (11) into account, we can express ψ_1 by

$$\psi_1 = \tan^{-1}\left(\frac{L_{\text{eff}}\omega_c - \left((1+\alpha)\times C_t\omega_c\right)^{-1}}{R_{\text{eff}}}\right). \tag{12}$$

From (3) and (12), the relation between $\tan(\psi_1)$ and $\tan(\psi_0)$ can be written as

$$\tan\left(\psi_1\right) = \tan\left(\psi_0\right) + \frac{\alpha}{(1+\alpha)\times C_t\omega_c R_{\text{eff}}}. \tag{13}$$

In an ASK-modulated system, MI is expressed by

$$\text{MI} = \frac{V_{L0} - V_{L1}}{V_{L0} + V_{L1}} \tag{14}$$

where V_{L0} and V_{L1} are the high and low amplitudes of the voltage across L_r, respectively. The output power of the Class-E transmitter is proportional to V_L^2; therefore, by considering (14), we can write

$$\frac{P_{\text{out}}\left(\psi_1\right)}{P_{\text{out}}\left(\psi_0\right)} = \left(\frac{V_{L1}}{V_{L0}}\right)^2 = \left(\frac{1-\text{MI}}{1+\text{MI}}\right)^2 \tag{15}$$

where $P_{\text{out}}(\psi_1)$ and $P_{\text{out}}(\psi_0)$ are the powers delivered to R_{ref} for the high and low modulation states, respectively. Substituting $\frac{P_{\text{out}}(\psi_1)}{P_{\text{out}}(\psi_0)}$ from (8) in (15), we arrive to

$$\exp\ \left(\tan\left(\psi_0\right) - \tan\left(\psi_1\right)\right) = \left(\frac{1-\text{MI}}{1+\text{MI}}\right)^2. \tag{16}$$

From (13) and (16), we can deduce

$$\exp\left(\frac{-\alpha}{(1+\alpha)\times C_{\rm t}\omega_{\rm c}R_{\rm eff}}\right)=\left(\frac{1-{\rm MI}}{1+{\rm MI}}\right)^2. \tag{17}$$

Finally, by reorganizing (17), we can calculate $C_{\rm m}$ using

$$C_{\rm m}=\ C_{\rm t}\times\left(\frac{-2\ln\left(\frac{1-{\rm MI}}{1+{\rm MI}}\right)}{\frac{1}{C_{\rm t}\omega_{\rm c}R_{\rm eff}}+2\ln\left(\frac{1-{\rm MI}}{1+{\rm MI}}\right)}\right). \tag{18}$$

Assuming that we need an MI of 10%, we substitute 0.1 for MI, 220 pF for $C_{\rm t}$, $2\pi\times10^7$ rad/s for $\omega_{\rm c}$ and 72.9 Ω for $R_{\rm eff}$ in (18), which results in $C_{\rm m}=\ 149.4$ pF.

The values of all the components in Fig. 3(b) have now been calculated other than the value of $V_{\rm DD}$. In an ideal Class-E PA, the power delivered to the load (PDL) can be found from (6). Therefore, if we know the required PDL, we can calculate the value of $V_{\rm DD}$.

In a practical Class-E power transmitter, the efficiency is considerably smaller than 100%. Some major sources of power loss in Fig. 3(b) are $R_{\rm Lt}$, $R_{\rm Lr}$, and M_1. In addition, some of the transmitted power is absorbed in the tissue. Therefore, the value of $V_{\rm DD}$ should be increased so that the desired amount of power is delivered to $R_{\rm L}$.

V. Simulation Results

We performed two sets of simulations. In the first set, we simulated Fig. 3(b), using ideal switches replacing M_1 and M_2. Our intent of this set of simulations was only to verify the accuracy of the proposed design procedure. As a result, to isolate the effects of the parasitic elements of the transistors on the proposed design procedure, we neglected these parasitic elements. In the second set of simulations, we simulated Fig. 3(b) using actual transistor models.

A. Simulation Results With Ideal Switches

We simulated Fig. 3(b) with the component values listed in Table II. The gate voltage ($V_{\rm G1}$), drain voltage ($V_{\rm D1}$), drain–source current ($I_{\rm M1}$), and the resonant current ($I_{\rm Lt}$) waveforms of M_1, when DATA is low, are plotted in Fig. 5(a). Clearly, $V_{\rm D1}$ satisfies ZVS and ZVDS conditions at the switch turn-on time. The same waveforms, when DATA is high, are plotted in Fig. 5(b).

Plotted in Fig. 6 is $V_{\rm L}$ when DATA is a random bit stream. When DATA is low, the amplitude of $V_{\rm L}$ is 9.29 V, which translates to a PDL of 52.8 mW. In this state, the drawn power from $V_{\rm DD}$ is 58.5 mW, meaning that the PTE of the link is 90.3%. When DATA is high, the amplitude of $V_{\rm L}$ is 7.62 V, which translates to a PDL of 35.5 mW. In this state, the drawn power from $V_{\rm DD}$ is 39.4 mW, meaning that the PTE of the link is 90.1%. As a result, the PTE is high in both modulation states. Moreover, the achieved MI is 9.9%, which matches well with the desired value of 10%, and validates the proposed design procedure.

Usually, in ASK-modulated Class-E power transmitters, the PTE is remarkably different if a bit ONE is transmitted compared with when a bit ZERO is transmitted; as a result, the PTE strongly depends on the data pattern. To properly measure the PTE, an actual (random) bit stream should be transmitted and the PDL should be divided over the dissipated power in the transmitter for a long bit stream. Moreover, often the transmitted data to the implant is encoded, for example, with 3b/6b, 4b/5b, or Manchester encoding, to avoid long runs of ONEs or ZEROs. We used PRBS-5 that does not have more than five ONEs or ZEROs in a row. We used the following formula to calculate PTE:

$$\text{PTE}\ =\frac{\frac{1}{NT}\int_0^{NT}\frac{V_{\rm L}^2(t)}{R_{\rm L}}dt}{P_{\rm TX}} \tag{19}$$

where T is the clock period and N is the number of clock cycles used for calculating the average PDL; $P_{\rm TX}$ represents the dissipated power in the transmitter and it includes the power drawn from $V_{\rm DD}$ and the power dissipated in the gate drivers. We kept $N>20$ to have a reasonable average of the power delivered to $R_{\rm L}$.

TABLE II
Specifications of the Simulated Class-E ASK Modulator Shown in Fig. 3(b), Using Ideal Switches

Component	Value	Comment
$V_{\rm DD}$	2.5 V	Supply voltage of the Class-E
$f_{\rm c}$	10 MHz	Carrier frequency
$L_{\rm RFC}$	6 μH	RF Choke of the Class-E
$C_{\rm p}$	79 pF	Parallel capacitor of the Class-E
$C_{\rm t}$	220 pF	Series capacitor of the Class-E
$C_{\rm m}$	149.4 pF	Modulation capacitor
$R_{\rm Lt}$	0.87 Ω	ESR of transmitter coil
$R_{\rm Lr}$	0.54 Ω	ESR of receiver coil
$R_{\rm L}$	817 Ω	Load resistance
$C_{\rm r}$	230.3 pF	Receiver resonance capacitor
k	0.21	Coupling coefficient
Elements	**Type**	**Comment**
M_1	Ideal Switch	Main Class-E Transistor
M_2	Ideal Switch	Modulation Transistor

B. Simulation With Actual Transistor Models

When we replace the ideal switches with actual transistor models, the Class-E power transmitter becomes untuned. We chose 2N7002BKW manufactured by Nexperia to realize M_1 and M_2. This transistor has a small output capacitance $C_{\rm o}$ of 7 pF, a small input capacitance $C_{\rm i}$ of 33 pF, an ON-resistance $R_{\rm on}$ of less than 2 Ω, and a drain–source breakdown voltage $V_{\rm BR(DSS)}$ of 60 V.

We performed the following procedure to design the circuit with actual transistor models. The procedure starts with designing and tuning the circuit shown in Fig. 1(a). We first calculate the initial values of the components using the design procedure explained in Section IV, and then fine-tuned the values of $C_{\rm p}$ and $C_{\rm t}$ using circuit simulation [22]. As a result of fine-tuning, the values of $C_{\rm p}$ and $C_{\rm t}$ changed to 64 and 250 pF, respectively.

We calculated $R_{\rm eff}$ using (4) and $C_{\rm m}$ using (18) which resulted in $C_{\rm m}=\ 212.6$ pF. We then constructed the circuit shown in Fig. 3(b). In Fig. 3(b), when M_2 is ON, $C_{\rm m}$ is placed between

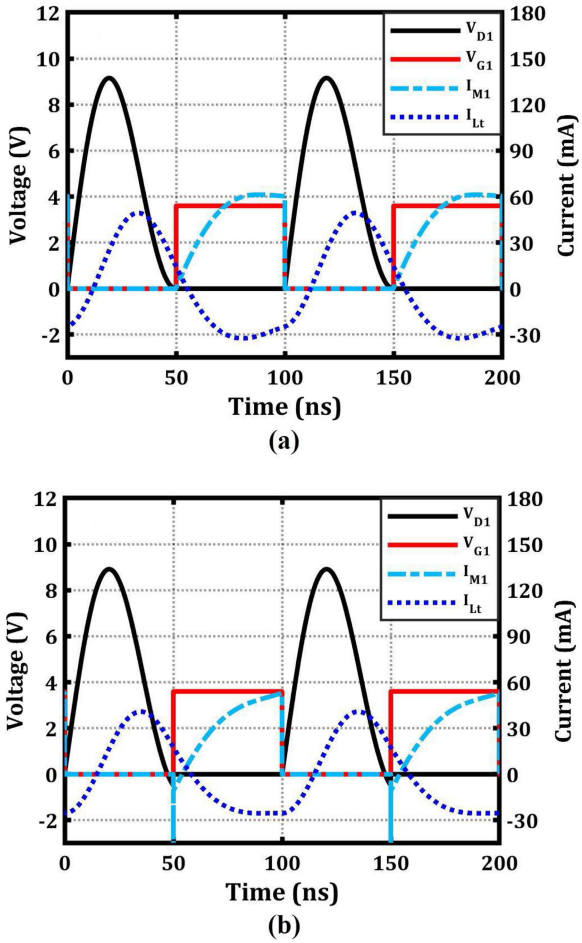

Fig. 5. Simulation results of Fig. 3(b) with ideal switches. (a) $V_{\rm D1}$, $V_{\rm G1}$, $I_{\rm M1}$, and $I_{\rm Lt}$ when DATA is low, (b) $V_{\rm D1}$, $V_{\rm G1}$, $I_{\rm M1}$, and $I_{\rm Lt}$ when DATA is high.

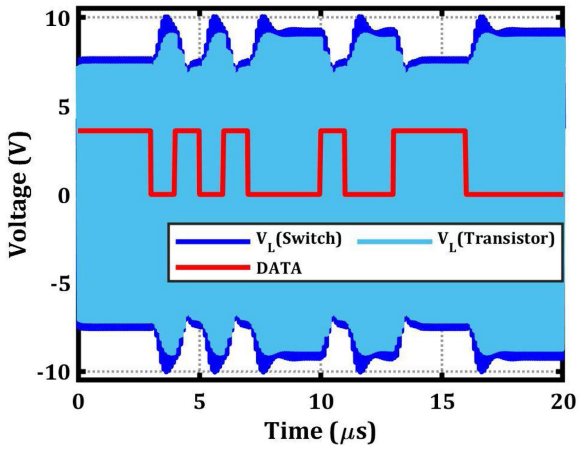

Fig. 6. Received signal across $R_{\rm L}$ ($V_{\rm L}$) when DATA is a random bit stream obtained from the simulation of Fig. 3(b) with ideal switches and actual transistor models.

node X and ground. On the other hand, when M_2 is OFF, the series connection of $C_{\rm m}$ and the output capacitance of M_2, i.e., $C_{\rm o2}$, is placed between node X and ground.

Ideally, $C_{\rm o2}$ should be zero and M_2 should be realized with a transistor that has a very small output capacitance compared with

TABLE III
SIMULATED AND IMPLEMENTED CLASS-E ASK MODULATOR SPECIFICATIONS

Component	SIMULATED	MEASURED
$V_{\rm DD}$	2.5 V	2.5 V
$f_{\rm c}$	10 MHz	10 MHz
$L_{\rm RFC}$	6.0 μH	5.7 μH
$C_{\rm p}$	60 pF	75 pF
$C_{\rm t}$	227.4 pF	244 pF
$C_{\rm m}$	235.2 pF	218 pF
$C_{\rm r}$	230.3 pF	235 pF
$R_{\rm L}$	817 Ω	817 Ω
PDL	37.6 mW	35 mW
PTE	68.4 %	64.6 %

TABLE IV
MAJOR SOURCES OF POWER LOSS IN THE SIMULATED CLASS-E ASK MODULATOR AND THEIR SHARE IN DEGRADING PTE

Major Sources of power loss	Degradation in PTE (%)
ESR of $L_{\rm t}$	1.00
ESR of $L_{\rm r}$	6.36
Power loss in M_1	6.97
Power loss in M_2	1.72
Gate drivers	15.55

$C_{\rm m}$. When M_2 is ON, $C_{\rm m}$ is placed in parallel to $C_{\rm t}$. In other words, the total capacitance between node X and ground is $C_{\rm t} + C_{\rm m}$. On the other hand, when M_2 is OFF, the series connection of $C_{\rm m}$ and $C_{\rm o2}$, which equals $C_{\rm m}\,C_{\rm o2}/(\,C_{\rm m} + C_{\rm o2})$, is placed between node X and ground, increasing the total capacitance from node X to ground to $C_{\rm t} + C_{\rm m}\,C_{\rm o2}/(\,C_{\rm m} + C_{\rm o2})$. In order to compensate for this side-effect of $C_{\rm o2}$, we should subtract $C_{\rm m}\,C_{\rm o2}/(\,C_{\rm m} + C_{\rm o2})$ from $C_{\rm t}$; however, because when M_2 is ON, $C_{\rm o2}$ is not seen, and the subtracted value should be added to $C_{\rm m}$.

We simulated Fig. 3(b) with actual transistor models in LTSPICE XVII. The values of the components resulted from the final simulation are reported in Table III. In our simulations, we used the 74HC245 gate as the gate driver, but we used MC74VHC04 manufactured by ON Semiconductor for the final prototype circuit. $V_{\rm D1}$, $V_{\rm G1}$, $I_{\rm M1}$, and $I_{\rm Lt}$, when DATA is low, are plotted in Fig. 7(a). Clearly, $V_{\rm D1}$ satisfies ZVS and ZVDS conditions. The same waveforms, for the case in which DATA is high, are plotted in Fig. 7(b).

When DATA is low, the amplitude of $V_{\rm L}$ is 8.78 V that translates to a PDL of 47.18 mW. In this state, the drawn power from $V_{\rm DD}$ is 56.82 mW and the dissipated power in the gate drivers is 8.5 mW. This results in an overall PTE of 72.2%. When DATA is high, the amplitude of $V_{\rm L}$ is 7.22 V, which translates to a PDL of 31.90 mW. In this state, the drawn power from $V_{\rm DD}$ is 38.76 mW, the dissipated power in the gate drivers is 8.6 mW, and the overall PTE is 67.4%.

The overall PDL and PTE, when a random 2-Mb/s bit stream is used, are 37.6 mW and 68.4% in simulation. The breakdown of major sources of power loss is reported in Table IV.

$V_{\rm L}$ for a random bit stream is plotted in Fig. 6. This plot is superimposed on the one resulted from simulation with ideal switches to highlight the difference. The measured MI in the

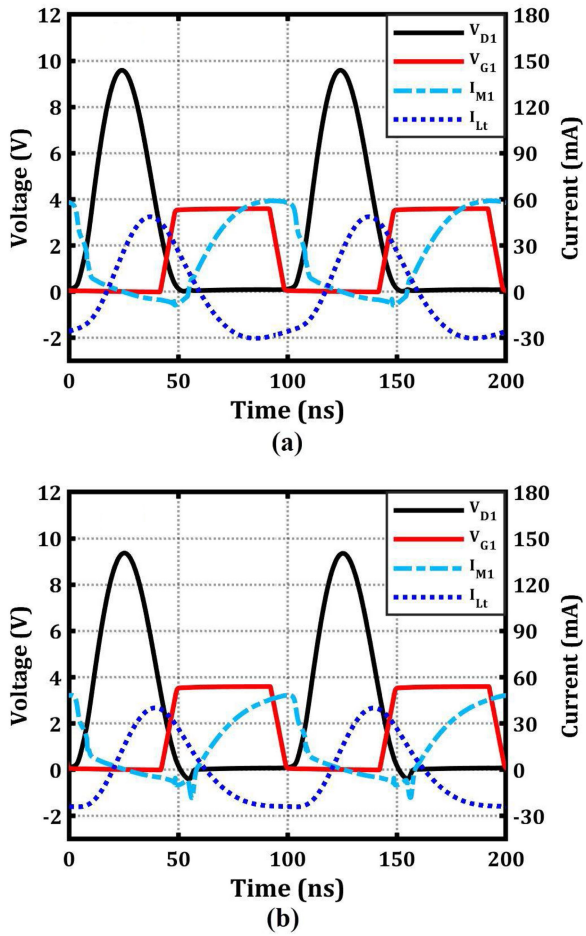

Fig. 7. Simulation results of Fig. 3(b) with actual transistor models. (a) $V_{\rm D1}$, $V_{\rm G1}$, $I_{\rm M1}$, and $I_{\rm Lt}$ when DATA is low, (b) $V_{\rm D1}$, $V_{\rm G1}$, $I_{\rm M1}$, and $I_{\rm Lt}$ when DATA is high.

simulation is 9.8%, which matches well with the desired value of 10%.

An advantage of the proposed circuit in this article is that the drawn power from $V_{\rm DD}$ of the Class-E transmitter is scaled according to PDL; as a result, PTE is maintained close to its peak value, no matter a bit ONE is transmitted or a bit ZERO. This is against what is observed in the conventional circuits, as in those, the power drawn from $V_{\rm DD}$ is mainly constant and ASK modulation is implemented in the transmitter by wasting power in a lossy device, such as a resistor or a Darlington transistor pair realizing the $V_{\rm DD}$ of the PA [20].

VI. Experimental Results

To prove the feasibility of the proposed circuit, we have implemented an inductive power and data transfer link using the proposed design procedure. The schematic of the implemented circuit is displayed in Fig. 8.

Usually, the receiver, i.e., the implant's circuitry, is integrated on a single or a few integrated circuits. However, since the focus and novelty of this work are on the transmitter rather than the receiver, we have implemented the receiver using commercial off-the-shelf components to only prove the feasibility of the proposed transmitter and verify its design procedure.

The receiver circuit, as shown in Fig. 8, includes $R_{\rm L}$, a half-wave voltage rectifier, and an ASK demodulator whose operation is explained later in this section.

The characterization of the link was performed in two steps. In the first step, switch $S_{\rm r}$ in Fig. 8 was in position 1 and the receiver was only a parallel *RLC* circuit, similar to the one shown in Fig. 3(b). In this step, we characterized the MI, PDL, and PTE of the link. The values of the components resulted from the experiment are reported in Table III. In the second step, switch $S_{\rm r}$ was in position 2, i.e., $R_{\rm L}$ was disconnected and the voltage rectifier and the ASK demodulator were connected to the receiver *LC* tank. In this step, we measured the BER of the link. Fig. 9 shows a photograph of the transmitter and receiver boards and the test setup.

A. First Characterization Step

In Fig. 10, $V_{\rm D1}$, $V_{\rm G1}$, and $I_{\rm M1}$ for the two modulation states are plotted. $I_{\rm M1}$ was plotted by measuring the voltage drop across a 1.2-Ω resistor inserted between the ground and the source of M_1. Fig. 10(a) is for the case that $DATA_{\rm in}$ is low and the Class-E transmitter is nominally tuned. Clearly, $V_{\rm D1}$ satisfies the ZVS and ZVDS conditions. Plotted in Fig. 10(b) is the same waveforms for the case that $DATA_{\rm in}$ is high.

$V_{\rm L}$ is shown in Fig. 11(a) and (b) for the data rate of 500 kb/s and 2 Mb/s, respectively. When $DATA_{\rm in}$ is low, the amplitude of $V_{\rm L}$ is 8.28 V that translates to a PDL of 41.96 mW. In this state, the drawn power from $V_{\rm DD}$ is 55.1 mW and the dissipated power in the gate drivers is about 8.1 mW. This results in an overall PTE of 66.4%.

When $DATA_{\rm in}$ is high, the amplitude of $V_{\rm L}$ is 6.76 V, which translates to a PDL of 27.97 mW. In this state, the drawn power from $V_{\rm DD}$ is 37.0 mW. The dissipated power in the gate drivers is about 8.1 mW. As a result, the overall PTE is 62.0%. As it is seen, the PTE is high in both modulation states. Moreover, the achieved MI is 10.11%, which matches well with the desired value of 10%.

To investigate the effect of the coil spacing, d, on MI, PDL, and PTE, we changed d and measured the resulting MI, PTE, and PDL without retuning the transmitter. Fig. 12 shows the PTE and PDL versus d. The maximum PTE was achieved when the transmitter was nominally tuned.

When we decrease d from 10 mm, we expect the PTE and PDL to increase due to the increase in the coupling coefficient; however, we observe that the PDL decreases but the PTE slightly increases but it then begins to decrease. The reason is that the reflected load from the receiver to the transmitter changes as d changes. As a result, when d decreases, the transmitter becomes slightly untuned, which itself results in the reduction of the PTE and PDL. On the other hand, when we increase the coil distance from 10 mm, $R_{\rm ref}$ decreases and $L_{\rm eff}$ increases due to the reduction in k. Therefore, as (3) indicates, the load network angles for low and high data bits move to the right side of the high-efficiency region, and as is seen in Fig. 2, $P_{\rm out}$ decreases.

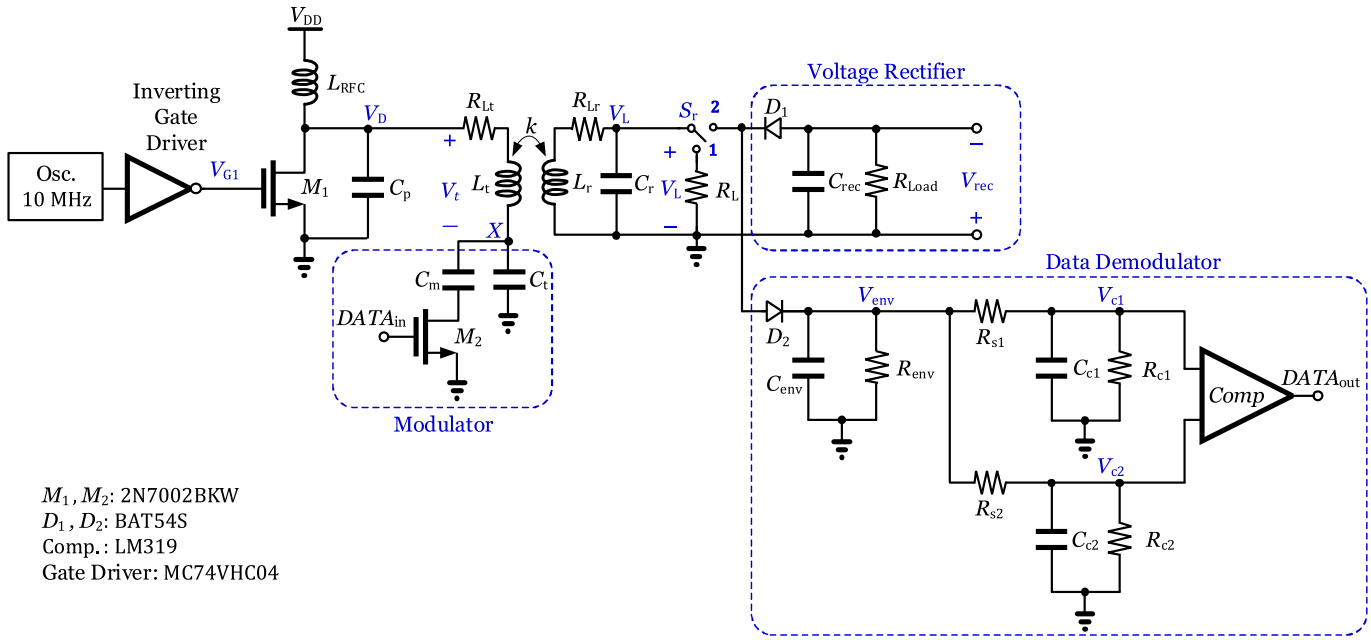

Fig. 8. Schematic of the prototyped wireless power and data transfer system, including Class-E transmitter, ASK modulator, half-wave rectifier, and ASK demodulator.

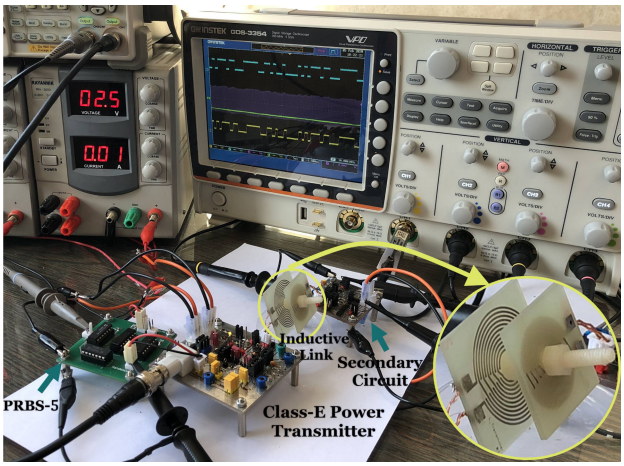

Fig. 9. Photograph of the experimental test setup.

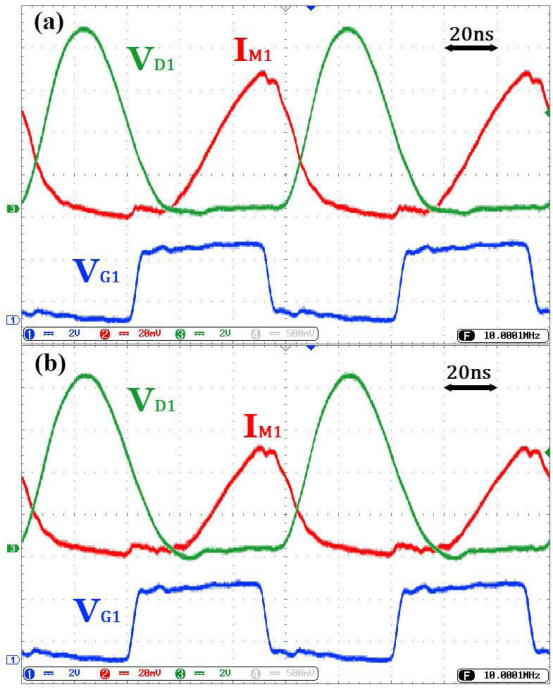

Fig. 10. Experimentally obtained gate voltage (V_{G1}), drain voltage (V_{D1}), and drain-source current (I_{M1}) waveforms of M_1. (a) When *DATA* is low, (b) When *DATA* is high. I_{M1} is the voltage drop across a 1.2-Ω resistor inserted between the source of M_1 and the ground.

Likewise PDL, PTE decreases due to the reduction in k as well as the detuning of the transmitter.

Fig. 13 shows the measured MI versus d. The measured MI, with $d = 10$ mm, is 10.1%, which matches well with the desired value of 10%. As d increases, R_{ref} decreases. This is well justified considering (17) into account. As is clear in Fig. 13, the MI changes considerably as the spacing between the coils changes. This weakness of the system is due to the fact that the power and the data transfer link is open-loop and there is no direct control on the MI on the receiver side; however, it should be noted that all open-loop inductive power and data transfer links suffer from this weakness.

B. Second Characterization Step

In this step, we removed R_{L} and put the half-wave rectifier and the ASK demodulator in the receiver circuit. In order to keep the power consumption in the receiver similar to the case that

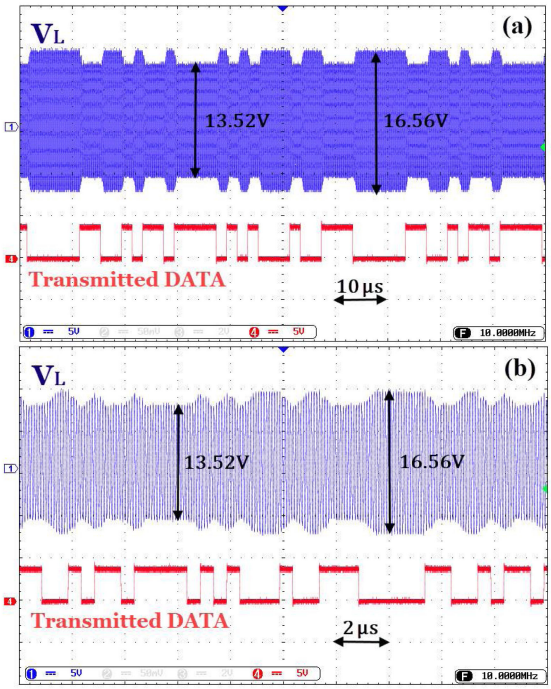

Fig. 11. Received signal across $R_{\rm L}$ ($V_{\rm L}$) when *DATA* is in the PRBS-5 format when the data rate is (a) 500 kb/s and (b) 2 Mb/s.

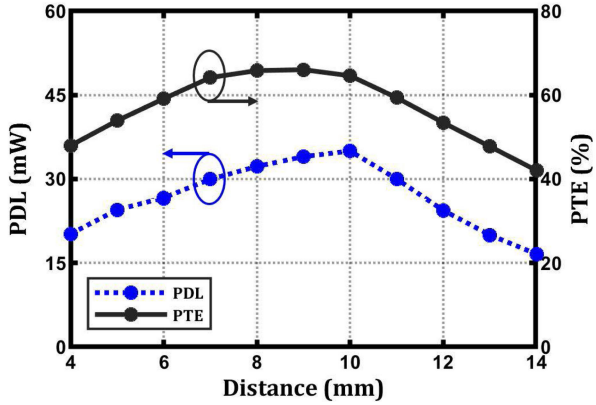

Fig. 12. Measured PTE and PDL versus coil distance. The result is for the case that the PA was tuned for the coil distance of 10 mm.

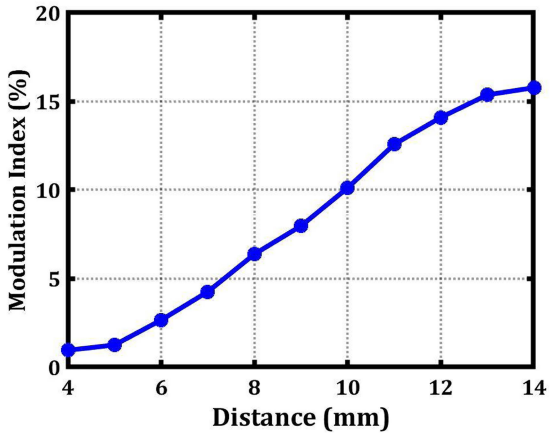

Fig. 13. Measured MI versus coil distance. The result is for the case that the PA was tuned for the coil distance of 10 mm.

only an 817-Ω resistor is connected to the receiver, the value of $R_{\rm Load}$ in the voltage rectifier was chosen to be 1.5 kΩ.

The half-wave rectifier rectifies the negative half-cycles of the received ac signals. The ASK demodulator detects the received data from the positive peaks. The ASK demodulator consists of an envelope detector, a comparator, and two low-pass filters (LPFs) with different cut-off frequencies. The envelope detector consisting of D_2, $C_{\rm env}$, and $R_{\rm env}$ extracts the envelope of the signal ($V_{\rm env}$). $V_{\rm env}$ is fed to the LPFs. The LPF consisting of $R_{\rm s1}$, $R_{\rm c1}$, and $C_{\rm c1}$ has a large time constant and extracts the average of the detected envelope signal. The LPF consisting of $R_{\rm s2}$, $R_{\rm c2}$, and $C_{\rm c2}$ has a smaller time constant and only smoothens the envelope signal. The comparator compares the outputs of these two filters and detects the received data bit.

To measure the BER of the link, we sent one billion pseudo-random bits generated by a PRBS-5 generator at data rates of 1 and 2 Mb/s. At the data rate of 1 Mb/s, the number of errors was zero; therefore, we can claim that the BER of the link is less than 10^{-8}. The measured BER at the data rate of 2 Mb/s was less than 10^{-6}.

Fig. 14(a)–(c) shows the input data ($DATA_{\rm in}$) to the transmitter, recovered data ($DATA_{\rm out}$) in the receiver, rectified voltage ($V_{\rm rec}$), and $V_{\rm r}$, which is the voltage across $L_{\rm r}$ for the data rates of 100 kb/s, 1 Mb/s, and 2 Mb/s, respectively. $DATA_{\rm out}$ truely matches $DATA_{\rm in}$. $V_{\rm rec}$ was measured to be 5.44, 5.38, and 5.32 V for the data rates of 100 kb/s, 1 Mb/s, and 2 Mb/s, respectively.

The MI of the received signals plotted in Fig. 14 is smaller than that of the ones plotted in Fig. 11 because of two reasons. First, the half-wave rectifier turns on at the negative peaks and cuts the amplitude of the negative half-cycles. This phenomenon inherently exists in any rectifier circuit as long as the rectifier capacitor $C_{\rm rec}$ is large. If a full-wave rectifier is used, both of positive and negative peaks are cut and the MI is reduced even more. To minimize this side-effect of the voltage rectifier, one can reduce $C_{\rm rec}$. In such case, the output voltage of the rectifier more closely follows the envelope of the induced signal on the receiver coil. Therefore, the same voltage rectifier can be used for voltage rectification as well as ASK demodulation. In that case, we observe a large variation (as large as MI) in the rectified voltage. To balance the trade-off between the fluctuations of the rectified voltage and the reduction of MI, we used two rectifiers: one extracts power from the negative peaks of the received ac signal, and one extracts data from the positive peaks.

The second reason for the reduction of MI is that when D_1 turns off, only a small load due to the data demodulator is connected across the receiver *LC* tank; therefore, the *q*-factor of the receiver *LC* tank momentarily increases, and as such, more carrier cycles are required for the signal envelope to settle to its final value.

Table V summarizes the measured specifications and compares them with those of the prior works in terms of data rate, PTE, PDL, and data-rate-to-carrier-frequency (DRCF) ratio.

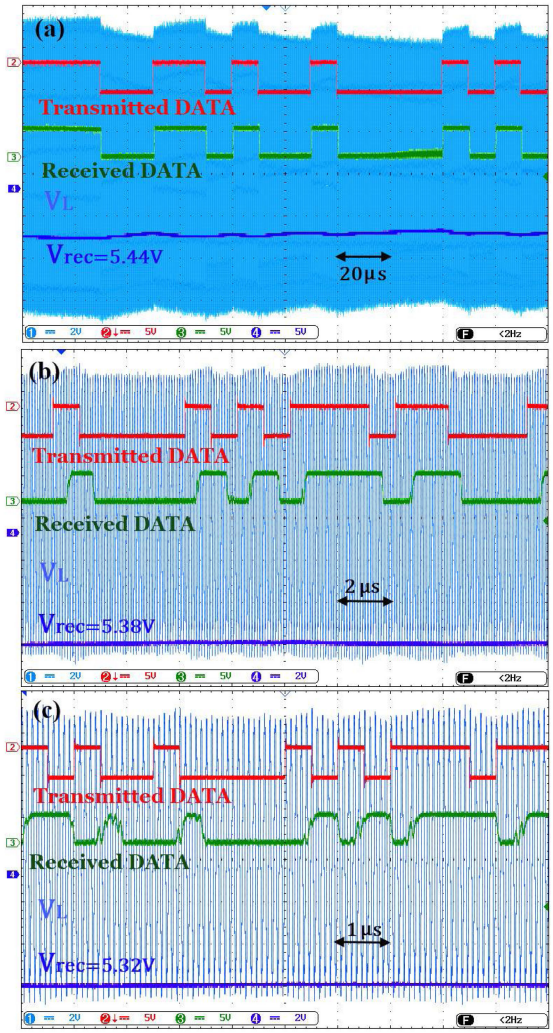

Fig. 14. Experimentally obtained waveforms of the implemented ASK modulator and demodulator when the data rate is (a) 100 kb/s, (b) 1 Mb/s, and (c) 2 Mb/s. From top: input bit stream, recovered data in the receiver, received analog ASK signal on the receiver coil, and the rectified voltage across R_{Load}.

TABLE V
COMPARISON WITH OTHER PUBLISHED POWER AND DATA TRANSFER LINKS

Publication	2008 [31]	2013 [32]	2018 [20]	2020 [30]	**This Work**	
Modulation Type	ASK	ASK	ASK	OOK	**ASK**	
Carrier Freq. (MHz)	8	5	10	2.5	**10**	
Data Rate (Mbps)	1	0.1	1	0.625	**1**	**2**
DRCF Ratio	0.125	0.02	0.1	0.25	**0.1**	**0.2**
BER	10^{-7}	-	10^{-5}	10^{-5}	$\mathbf{10^{-8}}$	$\mathbf{10^{-6}}$
Modulation index (%)	30*	31.46	10	100	**10**	**10**
Coupling Coefficient	-	-	0.32	-	**0.21**	**0.21**
Coils Distance (mm)	10	6	6	10	**10**	**10**
PDL (mW)	25	15	24	80	**35**	**35**
PTE (%)	60	4.4	52**	21	**65.4**	**64.6**

*Taken from Fig. 10 of the article presented in [31].
**Taken from Fig. 10(c) of the article presented in [20].

The presented power and data transfer links in this article outperform all the previously reported circuits in terms of PTE.

VII. SUMMARY

It is known that the efficiency of a Class-E PA or power transmitter is high in a range of load network angles. In this article, we proposed an ASK-modulated Class-E data and power transmitter, in which, both of its data modulation states operate in its high-efficiency region. Representing the load network angle with ψ, we showed that, in the range of $40^\circ < \psi < 65^\circ$, the output power of the Class-E transmitter is proportional to $\exp(-\tan(\psi))$. Taking advantage of this relation, we proposed an analytical design procedure for a Class-E power transmitter that drives an inductive power and data transfer link. We verified the proposed circuit and its design procedure in both simulation and measurement.

Using off-the-shelf components, we prototyped an inductive power and data transfer link based on the proposed transmitter. The link operates at a carrier frequency of 10 MHz and consists of a 2.4-µH transmitter coil and a 1.1-µH receiver coil separated by a 10-mm air gap. The measured PDL and PTE of the link are 35 mW and 64.6%, respectively. With an MI of 10%, the BER for the data rates of 1 and 2 Mb/s is less than 10^{-8} and 10^{-6}, respectively.

REFERENCES

[1] S.-Y. Lee *et al.*, "A programmable implantable microstimulator soc with wireless telemetry: Application in closed-loop endocardial stimulation for cardiac pacemaker," *IEEE Trans. Biomed. Circuits Syst.*, vol. 5, no. 6, pp. 511–522, Dec. 2011.
[2] P. Abiri *et al.*, "Inductively powered wireless pacing via a miniature pacemaker and remote stimulation control system," *Sci. Rep.*, vol. 7, no. 1, 2017, Art. no. 6180.
[3] J. F. Patrick, P. A. Busby, and P. J. Gibson, "The development of the nucleus freedom cochlear implant system," *Trends Amplification,* vol. 10, no. 4, pp. 175–200, 2006.
[4] F.-G. Zeng, S. Rebscher, W. Harrison, X. Sun, and H. Feng, "Cochlear implants: System design, integration, and evaluation," *IEEE Rev. Biomed. Eng.*, vol. 1, pp. 115–142, Nov. 2008.
[5] F.-G. Zeng *et al.*, "Development and evaluation of the nurotron 26-electrode cochlear implant system," *Hearing Res.*, vol. 322, pp. 188–199, 2015.
[6] N. Tran *et al.*, "A complete 256-electrode retinal prosthesis chip," *IEEE J. Solid-State Circuits*, vol. 49, no. 3, pp. 751–765, Mar. 2014.
[7] K. Chen, Z. Yang, L. Hoang, J. Weiland, M. Humayun, and W. Liu, "An integrated 256-channel epiretinal prosthesis," *IEEE J. Solid-State Circuits*, vol. 45, no. 9, pp. 1946–1956, Sep. 2010.
[8] M. Sivaprakasam, W. Liu, G. Wang, M. Zhou, J. D. Weiland, and M. S. Humayun, "Architecture trade-offs in high density microstimulators for retinal prosthesis," *IEEE Trans. Circuits Syst. I, Reg. Papers*, vol. 52, no. 12, pp. 2629–2641, Dec. 2005.
[9] M. Monge *et al.*, "A fully intraocular high-density self-calibrating epiretinal prosthesis," *IEEE Trans. Biomed. Circuits Syst.*, vol. 7, no. 6, pp. 747–760, Dec. 2013.
[10] H.-M. Lee, H. Park, and M. Ghovanloo, "A power-efficient wireless system with adaptive supply control for deep brain stimulation," *IEEE J. Solid-State Circuits*, vol. 48, no. 9, pp. 2203–2216, Sep. 2013.
[11] H.-M. Lee, K. Y. Kwon, W. Li, and M. Ghovanloo, "A power-efficient switched-capacitor stimulating system for electrical/optical deep brain stimulation," *IEEE J. Solid-State Circuits*, vol. 50, no. 1, pp. 360–374, Jan. 2015.
[12] V. Valente, C. Eder, N. Donaldson, and A. Demosthenous, "A high-power CMOS class-D amplifier for inductive-link medical transmitters," *IEEE Trans. Power Electron.*, vol. 30, no. 8, pp. 4477–4488, Aug. 2015.
[13] N. Donaldson, T. Perkins, I. Pachnis, A. Vanhoest, and A. Demosthenous, "Design of an implant for preventing incontinence after spinal cord injury," *Artif. Organs*, vol. 32, no. 8, pp. 586–591, 2008.
[14] X. Liu, A. Demosthenous, A. Vanhoestenberghe, D. Jiang, and N. Donaldson, "Active books: The design of an implantable stimulator that minimizes

cable count using integrated circuits very close to electrodes," *IEEE Trans. Biomed. Circuits Syst.*, vol. 6, no. 3, pp. 216–227, Jun. 2012.
[15] M. Ghovanloo and K. Najafi, "A wideband frequency-shift keying wireless link for inductively powered biomedical implants," *IEEE Trans. Circuits Syst. I, Reg. Papers*, vol. 51, no. 12, pp. 2374–2383, Dec. 2004.
[16] M. M. Ahmadi and S. Ghandi, "A Class-E power amplifier with wideband FSK modulation for inductive power and data transmission to medical implants," *IEEE Sensors J.*, vol. 18, no. 17, pp. 7242–7252, Sep. 2018.
[17] I. A. Mashhadi, M. Pahlevani, S. Hor, H. Pahlevani, and E. Adib, "A new wireless power-transfer circuit for retinal prosthesis," *IEEE Trans. Power Electron.*, vol. 34, no. 7, pp. 6425–6439, Jul. 2019.
[18] M. K. Kazimierczuk, *Radio-Frequency Power Amplifiers*, 2nd ed. New York, NY, USA: Wiley, 2015.
[19] B. Ziaie, S. C. Rose, M. D. Nardin, and K. Najafi, "A self-oscillating detuning-insensitive Class-E transmitter for implantable microsystems," *IEEE Trans. Biomed. Eng.*, vol. 48, no. 3, pp. 397–400, Mar. 2001.
[20] M. L. Navaii, H. Sadjedi, and A. Sarrafzadeh, "Efficient ASK data and power transmission by the Class-E with a switchable tuned network," *IEEE Trans. Circuits Syst. I, Reg. Papers*, vol. 65, no. 10, pp. 3255–3266, Oct. 2018.
[21] F. H. Raab, "Effects of circuit variations on the class E tuned power amplifier," *IEEE J. Solid-State Circuits*, vol. 13, no. 2, pp. 239–247, Apr. 1978.
[22] N. O. Sokal, "Class-E RF power amplifiers," QEX, 2001.
[23] F. H. Raab, "Recollections of Nathan Sokal: The man, his work, and the Class-E amplifier," *IEEE Microw. Mag.*, vol. 19, no. 5, pp. 16–21, Jul./Aug. 2018.
[24] R. R. Harrison, "Designing efficient inductive power links for implantable devices," in *Proc. IEEE Int. Symp. Circuits Syst.*, 2007, pp. 2080–2083.
[25] M. Kazimierczuk, "Collector amplitude modulation of the class E tuned power amplifier," *IEEE Trans. Circuits Syst.*, vol. 31, no. 6, pp. 543–549, Jun. 1984.
[26] J. Sacristan, F. Segura, and M. T. Oses, "Bidirectional telemetry for implantable systems," in *Proc. IEEE Int. Symp. Circuits Syst.*, 2006, pp. 349–352.
[27] Y. Hu and M. Sawan, "A fully integrated low-power BPSK demodulator for implantable medical devices," *IEEE Trans. Circuits Syst. I, Reg. Papers*, vol. 52, no. 12, pp. 2552–2562, Dec. 2005.
[28] U.-M. Jow and M. Ghovanloo, "Modeling and optimization of printed spiral coils in air, saline, and muscle tissue environments," *IEEE Trans. Biomed. Circuits Syst.*, vol. 3, no. 5, pp. 339–347, Oct. 2009.
[29] P. R. Troyk and M. A. K. Schwan, "Closed-loop class e transcutaneous power and data link for microimplants," *IEEE Trans. Biomed. Eng.*, vol. 39, no. 6, pp. 589–599, Jun. 1992.
[30] M. M. Ahmadi and M. Sarbandi-Farahani, "A Class-E power and data transmitter with on–off keying data modulation for wireless power and data transmission to medical implants," *Circuits, Syst., Signal Process.*, vol. 39, pp. 4174–4186, 2020.
[31] J. Sacristan-Riquelme, F. Segura, and M. T. Osés, "Simple and efficient inductive telemetry system with data and power transmission," *Microelectron. J.,* vol. 39, no. 1, pp. 103–111, 2008.
[32] J. Olivo, S. Carrara, and G. De Micheli, "A study of multi-layer spiral inductors for remote powering of implantable sensors," *IEEE Trans. Biomed. Circuits Syst.*, vol. 7, no. 4, pp. 536–547, Aug. 2013.

Mohammad Mahdi Ahmadi (Senior Member, IEEE) received the B.Sc. degree in biomedical engineering (highest hons.) from Shahid Beheshti University, Tehran, Iran, in 2000, the M.Sc. degree in electronic engineering from Sharif University of Technology, Tehran, Iran, in 2002, and the Ph.D. degree in electrical engineering from the University of Calgary, Calgary, AB, Canada, in 2007.

His Ph.D. research was on developing a wireless implantable microsystem for continuous blood glucose monitoring. From 2007 to 2010, he was with Sound Design Technologies, Ltd., Burlington, Canada (acquired by ON Semiconductor), where he designed ultra low-power power and low-voltage analog integrated circuits for hearing aids. From 2010 to 2014, he was with Synopsys, Inc., Toronto, Canada, where he designed high-speed circuits for multistandard multi-Gb/s wireline applications. In the Summers of 2015–2017, he was with Rambus, Inc., Sunnyvale, USA, and in the Summers from 2018 to 2021, he was with Analog Bits, Inc., Sunnyvale, USA, designing high-speed wireline circuits. Since 2014, he has been an Assistant Professor with the Department of Biomedical Engineering, Amirkabir University of Technology, Tehran, Iran. His current research interests include biomedical circuits and systems.

Dr. Ahmadi was the winner of the 44th ISSCC/DAC Student Design Contest in the Operational Chip category, in 2007. He was part of a team that received the 2010 EDN Innovation Award for developing the world's first full SoC for hearing aids**.**

Shirin Pezeshkpour (Student Member, IEEE) received the B.Sc. (hons.) and M.Sc. (hons.) degrees in biomedical engineering, in 2017 and 2019, respectively, from Amirkabir University of Technology (Tehran Polytechnic), Tehran, Iran, where she is currently working toward the Ph.D. degree in biomedical engineering.

Her research interests focus on the circuit design for biomedical applications, specifically high-efficiency wireless data and power transfer systems for medical implants.

Zahra Kabirkhoo (Student Member, IEEE) received the dual B.Sc. degrees in biomedical and electrical engineering and the M.Sc. degree in biomedical engineering from Amirkabir University of Technology, Tehran, Iran, in 2016 and 2018, respectively. She is currently working toward the Ph.D. degree in electrical engineering at the University of Calgary, Calgary, AB, Canada.

Her M.Sc. thesis focused on the wireless power and data transmission to medical implants. Her current research interest focuses on the mixed-signal integrated circuits, specifically high-speed analog-to-digital converters.